5466 *Chem. Mater.* **2009,** *21,* 5466–5473
DOI:10.1021/cm902626z

CHEMISTRY OF MATERIALS
Article

Ordered Three- and Five-ply Nanocomposites from ABC Block Terpolymer Microphase Separation with Niobia and Aluminosilicate Sols

Morgan Stefik,[†] Surbhi Mahajan,[†,‡] Hiroaki Sai,[†] Thomas H. Epps, III,[§,⊥] Frank S. Bates,[§] Sol M. Gruner,[∥,○] Francis J. DiSalvo,[#] and Ulrich Wiesner*[,†]

[†]*Materials Science and Engineering, Cornell University, Ithaca, New York 14853,* [§]*Department of Chemical Engineering and Materials Science, University of Minnesota, Minneapolis, Minnesota 55455,* [∥]*Department of Physics, Cornell University, Ithaca, New York 14853,* [○]*Cornell High Energy Synchrotron Source, Cornell University, Ithaca, New York 14853, and* [#]*Department of Chemistry and Chemical Biology, Cornell University, Ithaca, New York 14853.* [‡]*Present address: DuPont Central Research and Development, Experimental Station, Route 141 and Henry Clay, Wilmington, Delaware 19880-0328.* [⊥]*Present address: Department of Chemical Engineering, University of Delaware, Newark, Delaware 19716.*

Received August 25, 2009. Revised Manuscript Received September 24, 2009

We report the first use of a nonfrustrated block terpolymer for the synthesis of highly ordered oxide nanocomposites containing multiple plies. The morphological behavior of 15 ISO-oxide nanocomposites was investigated spanning a large range of compositions along the $f_I = f_S$ isopleth using aluminosilicate and niobia sols. Morphologies were determined by transmission electron microscopy (TEM) and small-angle X-ray scattering (SAXS) measurements. Four morphologies were identified, including core−shell hexagonal, core−shell double gyroid, three-domain lamellae, and core−shell inverse-hexagonal, in order of increasing O + oxide volume fraction. All of the resulting nanocomposites had three- or five-ply morphologies containing domains that were continuous in one, two, or three dimensions. The five-ply core−shell double gyroid phase was only found to be stable when the O + oxide domain was a minority. Removal of the polymer enabled simple and direct synthesis of mesoporous oxide materials while retaining the ordered network structure. We believe that advances in the synthesis of multiply nanocomposites will lead to advanced materials and devices containing multiple plies of functional materials.

Introduction

The microphase separation of amphiphilic block copolymers has been broadly applied toward structure-direction in numerous materials. Typically, the hydrophilic block is selectively swelled with hydrophilic particles via attractive intermolecular forces while the hydrophobic block is repelled. The balance of interface and chain stretching free energies leads the polymer to direct the coassembly into various ordered morphologies. While such techniques have been extensively studied with diblock (AB)[1] and triblock (ABA) copolymers,[2,3] there are very few examples of triblock terpolymers (ABC) used as structure-directing agents.[4−6]

The application of triblock terpolymers as structure-directing agents is particularly interesting due to the dozens of known ordered morphologies of the neat polymers.[7−17] The plethora of network morphologies[18] is especially applicable to devices, such as fuel cells, batteries, or supercapacitor electrodes, which require multiple transport materials arranged in continuous pathways for fuel/electrolyte, ion conduction/storage, and electron transport. The network phases formed by triblock terpolymers are not only trifunctional, but also form over a

*Corresponding author. E-mail: ubw1@cornell.edu.

(1) Templin, M.; Franck, A.; DuChesne, A.; Leist, H.; Zhang, Y. M.; Ulrich, R.; Schadler, V.; Wiesner, U. *Science* **1997**, *278*(5344), 1795–1798.
(2) Yang, P. D.; Zhao, D. Y.; Margolese, D. I.; Chmelka, B. F.; Stucky, G. D. *Nature* **1998**, *396*(6707), 152–155.
(3) Zhao, D. Y.; Feng, J. L.; Huo, Q. S.; Melosh, N.; Fredrickson, G. H.; Chmelka, B. F.; Stucky, G. D. *Science* **1998**, *279*(5350), 548–552.
(4) Epps, T. H.; Bailey, T. S.; Waletzko, R.; Bates, F. S. *Macromolecules* **2003**, *36*(8), 2873–2881.
(5) Toombes, G. E. S.; Mahajan, S.; Thomas, M.; Du, P.; Tate, M. W.; Gruner, S. M.; Wiesner, U. *Chem. Mater.* **2008**, *20*(10), 3278–3287.
(6) Toombes, G. E. S.; Mahajan, S.; Weyland, M.; Jain, A.; Du, P.; Kamperman, M.; Gruner, S. M.; Muller, D. A.; Wiesner, U. *Macromolecules* **2008**, *41*(3), 852–859.
(7) Mogi, Y.; Kotsuji, H.; Kaneko, Y.; Mori, K.; Matsushita, Y.; Noda, I. *Macromolecules* **1992**, *25*(20), 5408–5411.
(8) Auschra, C.; Stadler, R. *Macromolecules* **1993**, *26*(9), 2171–2174.
(9) Krappe, U.; Stadler, R.; Voigtmartin, I. *Macromolecules* **1995**, *28*(13), 4558–4561.
(10) Zheng, W.; Wang, Z.-G. *Macromolecules* **1995**, *28*(21), 7215–7223.
(11) Matsushita, Y.; Suzuki, J.; Seki, M. In *Surfaces of tricontinuous structure formed by an ABC triblock copolymer in bulk*; Elsevier Science Bv: New York, 1998; pp 238−242.
(12) Shefelbine, T. A.; Vigild, M. E.; Matsen, M. W.; Hajduk, D. A.; Hillmyer, M. A.; Cussler, E. L.; Bates, F. S. *J. Am. Chem. Soc.* **1999**, *121*(37), 8457–8465.
(13) Bates, F. S.; Fredrickson, G. H. *Phys. Today* **1999**, *52*(2), 32–38.
(14) Bailey, T. S.; Hardy, C. M.; Epps, T. H.; Bates, F. S. *Macromolecules* **2002**, *35*(18), 7007–7017.
(15) Ludwigs, S.; Boker, A.; Abetz, V.; Muller, A. H. E.; Krausch, G. *Polymer* **2003**, *44*(22), 6815–6823.
(16) Walther, A.; Goldel, A.; Muller, A. H. E. *Polymer* **2008**, *49*(15), 3217–3227.
(17) Jinnai, H.; Kaneko, T.; Matsunaga, K.; Abetz, C.; Abetz, V. *Soft Matter* **2009**, *5*(10), 2042–2046.
(18) Bates, F. S. *MRS Bull.* **2005**, *30*(7), 525–532.

 Published on Web 10/21/2009

much wider phase composition window (4−14.1 vol %[14,19]) than the bifunctional double gyroid structure found in diblock copolymer systems (2−6 vol %[20]). Such a method of fabrication, where a sequence of three or more unique polymer blocks direct the spatial arrangement of multiple materials, thus defining the interfaces and pathways, is termed block sequence directed materials (BSDMs).[21] The achievement of BSDMs would be a significant advance toward mimicking the complex assembly processes apparent in nature. In particular, ordered transition metal oxide materials are interesting in energy generation, storage, and conversion applications due to their ability to catalyze reactions, conduct ions, and intercalate ions.[22,23] Indeed, it has already been shown that the three blocks of a terpolymer can be designed to lead to trifunctional materials with control over each of the three final components.[21]

Morphology prediction of triblock terpolymer coassemblies is particularly complex due to the number of parameters. The phase behavior of ideal diblock copolymers may be predicted solely based on two parameters: the volume fraction f_a of the A block and the product χN of Flory−Huggins χ parameter with the overall degree of polymerization N. In contrast, the phase behavior of ideal triblock terpolymers is governed by five parameters: two independent volume fractions, f_a and f_b, and the products of three Flory−Huggins parameters, $\chi_{AB}N$, $\chi_{BC}N$, and $\chi_{AC}N$. The relative magnitude of each of the χ parameters further determines the types of morphologies formed. When χ_{AC} is the largest, the system is considered nonfrustrated[24] and the large energetic penalty of A−C contacts leads to only core−shell and alternating versions of the morphologies found in diblock copolymers.[19] In contrast, frustrated block terpolymers are known to form decorated morphologies in which A−C interfaces are made to minimize A−B or B−C interfaces.[25] This morphological tendency was preserved when aluminosilicate structures were directed with such frustrated triblock terpolymers.[5,6]

The symmetry of the polymer blocks, or lack thereof, influences interfacial curvature. Symmetric and near symmetric diblock copolymers ($f_a \approx f_b$) form lamellar morphologies whereas asymmetric diblock copolymers lead to morphologies with curved interfaces, including gyroid, hexagonal cylinders, and cubic micellar phases. Similarly, triblock terpolymer morphologies are influenced by both the A−B and B−C symmetries. Symmetric−symmetric ideal triblock terpolymers ($f_a = f_b = f_c$) form a three-domain lammelae phase with flat interfaces whereas asymmetric-asymmetric triblock terpolymers ($f_a \neq f_b \neq f_c$) form numerous morphologies with curved interfaces. Combining both of these tendencies with a symmetric−asymmetric triblock terpolymer ($f_a = f_b \neq f_c$) can cause the competing interfacial forces to buckle the interface into periodic networks of saddle surfaces.[26]

Herein, we present the results from the use of a nonfrustrated, symmetric−asymmetric triblock terpolymer as a structure directing agent for oxide materials. To the best of our knowledge, this is the first report of ordered oxide materials structure-directed by a nonfrustrated block terpolymer.

Experimental Methods

Materials Synthesis. The poly(isoprene-*b*-styrene-*b*-ethylene oxide) (ISO) triblock terpolymers used here were prepared by sequential anionic polymerization and were thoroughly characterized previously.[14] ISO3 had a molecular weight of 15.24 kg/mol and a polydispersity of 1.05. ISO4 had a molecular weight of 15.78 kg/mol and a polydispersity of 1.05. The volume fractions of I, S, and O were calculated based on reported homopolymer densities at 140 °C.[27] The volume fractions of I, S, and O in ISO3 were determined to be 0.448, 0.454, and 0.098, respectively. Similarly, ISO4 had volume fractions of 0.440, 0.435, and 0.125 for I, S, and O, respectively. The equilibrium morphologies of ISO3 and ISO4 were previously determined to be two-domain lamellar and O^{70}, respectively.[14] The O^{70} is a tricontinuous orthorhombic network structure which was first identified in 2002 and has been detailed elsewhere.[14,18,26,28] ISO polymers are amphiphilic, having a hydrophilic O block and two hydrophobic blocks, I and S. The hydrophilic oxide sol particles are expected to selectively swell the O block.

Each aluminosilicate hybrid film was prepared from a 2.0−2.5 wt % polymer solution in THF−$CHCl_3$ (1:1 by volume) by adding a predetermined amount of aluminosilicate sol solution and casting the homogeneous mixture covered at 60 °C. The sol solution was prepared using a two step acid catalyzed hydrolysis procedure as described in detail elsewhere.[1,29] This sol is an organically modified ceramic (ORMOCER) which has much lower density than bulk silica.[1,30] The volume fraction of the combined O and aluminosilicate phase was calculated using a combined density of 1.4 g/cm^3 as thoroughly established previously.[5,6,31−34]

(19) Tyler, C. A.; Qin, J.; Bates, F. S.; Morse, D. C. *Macromolecules* **2007**, *40*(13), 4654–4668.
(20) Floudas, G.; Ulrich, R.; Wiesner, U. *J. Chem. Phys.* **1999**, *110*(1), 652–663.
(21) Stefik, M.; Sai, H.; Sauer, K.; Gruner, S. M.; DiSalvo, F. J.; Wiesner, U. *Macromolecules* **2009**, *42*(17), 6682–6687.
(22) Crossland, E. J. W.; Kamperman, M.; Nedelcu, M.; Ducati, C.; Wiesner, U.; Smilgies, D. M.; Toombes, G. E. S.; Hillmyer, M. A.; Ludwigs, S.; Steiner, U.; Snaith, H. J. *Nano Lett.* **2008**, *9*, 2807–2812.
(23) Stefik, M.; Lee, J.; Wiesner, U. *Chem. Commun.* **2009**, *18*, 2532–2534.
(24) Bailey, T. S. Morphological behavior spanning the symmetric AB and ABC block copolymer states. Thesis, University of Minnesota, **2001**.
(25) Bailey, T. S.; Pham, H. D.; Bates, F. S. *Macromolecules* **2001**, *34* (20), 6994–7008.
(26) Epps, T. H.; Cochran, E. W.; Bailey, T. S.; Waletzko, R. S.; Hardy, C. M.; Bates, F. S. *Macromolecules* **2004**, *37*(22), 8325–8341.
(27) Fetters, L. J.; Lohse, D. J.; Richter, D.; Witten, T. A.; Zirkel, A. *Macromolecules* **1994**, *27*(17), 4639–4647.
(28) Chatterjee, J.; Jain, S.; Bates, F. S. *Macromolecules* **2007**, *40*(8), 2882–2896.
(29) Warren, S. C.; Disalvo, F. J.; Wiesner, U. *Nat. Mater.* **2007**, *6*(3), 248–248.
(30) Simon, P. F. W.; Ulrich, R.; Spiess, H. W.; Wiesner, U. *Chem. Mater.* **2001**, *13*(10), 3464–3486.
(31) Finnefrock, A. C.; Ulrich, R.; Toombes, G. E. S.; Gruner, S. M.; Wiesner, U. *J. Am. Chem. Soc.* **2003**, *125*(43), 13084–13093.
(32) Jain, A.; Toombes, G. E. S.; Hall, L. M.; Mahajan, S.; Garcia, C. B. W.; Probst, W.; Gruner, S. M.; Wiesner, U. *Angew. Chem., Int. Ed.* **2005**, *44*(8), 1226–1229.
(33) Jain, A.; Hall, L. M.; Garcia, C. B. W.; Gruner, S. M.; Wiesner, U. *Macromolecules* **2005**, *38*(24), 10095–10100.
(34) Cho, B. K.; Jain, A.; Gruner, S. M.; Wiesner, U. *Chem. Mater.* **2007**, *19*(15), 3611–3614.

Each niobia hybrid film was prepared from a 0.3−0.8 wt % polymer solution in $CHCl_3$ by forming a nonhydrolytic sol in situ, in a similar fashion to that previously described.[35] Specifically, niobium(V) ethoxide was added to the stirring polymer solution in a nitrogen glovebox. After 10 min of stirring, niobium(V) chloride was added in a 1.0:1.61 chloride:ethoxide molar ratio. The polymer−sol solution was stirred overnight at room temperature and cast in a Teflon dish at 50 °C covered with a glass hemisphere. All films were subsequently placed in a vacuum oven at 130 °C for at least 1 h. The volume fraction of the O and niobia containing domain was calculated using densities of 1.064 and 2.0 g/cm^3, respectively. We believe that this is a reasonable estimate for the density of the amorphous niobia sol since metal oxide sol−gel densities are often less than half that of the bulk density.[36]

Transmission Electron Microscopy (TEM). Ultrathin sections were cut at −55 °C using a Leica Ultracut UCT microtome. The sections were transferred to copper grids and stained with aqueous 2 wt % OsO_4 solution or anhydrous OsO_4 vapor. Staining made the poly(isoprene) darker than poly(styrene). Bright field TEM was performed on a Tecnai T12 operating at 120 kV. The ISO polymer was removed from a sectioned sample by using a Fischione model 1020 Ar−O plasma cleaner. The 10 min etching time combined with a ∼1 nm/s carbon etch rate was sufficient to remove all of the ISO from the c.a. 70 nm thick sections.

Small Angle X-ray Scattering (SAXS). A Rigaku RU300 with a copper rotating anode (λ = 1.54 Å) operated at 40 kV and 50 mA was used to gather SAXS data of the niobia containing samples. The X-rays were monochromated and focussed with a Ni filter and orthogonal Franks mirrors. The 2D scattering patterns were collected with a home-built 1000 × 1000 pixel CCD detector similar to that described elsewhere.[37] SAXS data of the aluminosilicate containing samples were collected at the Cornell High Energy Synchrotron Source (CHESS), with a setup consisting of a multilayer monochromator (λ = 1.457 Å) with a 2D area detector and a sample-to-detector distance of 1.61 m. Data are presented as 1D plots of radially integrated intensity versus scattering vector q where $q = 4\pi \sin(\theta)\lambda^{-1}$, where 2θ is the total scattering angle.

Results

Aluminosilicate Nanocomposites. Our initial experiments targeted the orthorhombic O^{70} network phase. A previous study showed that neat ISO polymers along the $f_I = f_S$ isopleth form the O^{70} phase over a wide composition window spanning from 9.8 to 23.9 vol % of O.[14] We synthesized six nanocomposites within this window spanning from 15 to 23 vol % O + oxide. The stained TEM images of five of these nanocomposites ranging from 15.0 to 22.3 vol % O + oxide were characteristic of a core−shell hexagonal morphology (CS-H) containing O + oxide cores (gray) covered by a S shell (light) within an I matrix (dark) (Figure 1A). The two samples with the least amount of oxide, ISO3-S1 and ISO4-S1, were primarily composed of short-range ordered wormlike structures, but ISO4-S1 also had some well-ordered CS-H regions. The SAXS patterns of these CS-H nanocomposites were also consistent with hexagonal symmetry, exhibiting characteristic peaks in the ratios defined as $q/q^* = 1$, $\sqrt{3}$, and $\sqrt{7}$ (Figure 2A). The d_{10} spacing for this series of samples varied from 19.9 to 22.2 nm and were consistent with the molecular weight of the ISO polymers as well as the observed c.a. 20 nm cylinder spacings in TEM (Table I).

The three aluminosilicate samples with the highest O + oxide compositions all had similar phase behavior. TEM images of all three of these samples, ISO3-S4, ISO4-S3, and ISO4-S4, ranging from 23.0 to 32.3 vol % O + oxide exhibited core−shell wagon-wheel patterns with silicate cores (gray) surrounded by a S shell (light) within an I matrix (dark) which were characteristic of the (111) plane of the core−shell double gyroid (CS-G^D) morphology (Figure 1B). The CS-G^D phase is a pentacontinuous structure with two separate core−shell gyroid networks of the same composition. Other TEM images of these samples were consistent with the (100) (Figure 1B inset) and (125) projections of the CS-G^D. The SAXS patterns of these samples were also consistent with the CS-G^D morphology exhibiting the strongest scattering at $q/q^* = \sqrt{6}$, followed by peaks consistent with $\sqrt{8}$, $\sqrt{14}$, $\sqrt{16}$, $\sqrt{20}$, and $\sqrt{22}$ (Figure 2B). Samples ISO4-S3 and ISO4-S4 also exhibited a small peak corresponding to a forbidden reflection at $\sqrt{2}q^*$. Such forbidden reflections were also observed in previous cocontinuous cubic silica-type structures which were compressed in the z-direction leading to a breaking of the symmetry of the cubic phases.[22,31,38−40] The CS-G^D nanocomposites in this study were all made by solvent casting which is well-known to compress films in the direction of evaporation. A 2D SAXS pattern of ISO4-S4 perpendicular to the evaporation direction (data not shown) showed 3.6−14.2% compression (varies from grain to grain) of the $\sqrt{6}q^*$ ring and is attributed to the appearance of the forbidden reflection at $\sqrt{2}q^*$. The d_{100} spacing determined by SAXS ranged from 52.9 to 56.2 nm and was consistent with the observed 53−63 nm spacings observed in TEM. The roughly twice as large lattice dimension, d, for CS-G^D relative to the CS-H is due to the pentacontinuous nature of the CS-G^D morphology which has twice as many interfaces per unit cell: O−S−I−I−S−O−O−S−I−I−S−O compared to O−S−I−I−S−O. Thus, the much larger lattice dimension d is still consistent with the molecular weight of the ISO polymers used. Sample ISO4-S4 with the largest amount of O + oxide fraction of 32.3 vol % had c.a. 20% three-domain lamellae (Lam$_3$) phase and is thus very close to Lam$_3$ phase space.

(35) Lee, J.; Orilall, M. C.; Warren, S. C.; Kamperman, M.; Disalvo, F. J.; Wiesner, U. *Nat. Mater.* **2008**, *7*(3), 222–228.
(36) Alberius, P. C. A.; Frindell, K. L.; Hayward, R. C.; Kramer, E. J.; Stucky, G. D.; Chmelka, B. F. *Chem. Mater.* **2002**, *14*(8), 3284–3294.
(37) Tate, M. W.; Eikenberry, E. F.; Barna, S. L.; Wall, M. E.; Lowrance, J. L.; Gruner, S. M. *J. Appl. Crystallogr.* **1995**, *28*, 196–205.
(38) Klotz, M.; Albouy, P. A.; Ayral, A.; Menager, C.; Grosso, D.; Van der Lee, A.; Cabuil, V.; Babonneau, F.; Guizard, C. *Chem. Mater.* **2000**, *12*(6), 1721–1728.
(39) Toombes, G. E. S.; Finnefrock, A. C.; Tate, M. W.; Ulrich, R.; Wiesner, U.; Gruner, S. M. *Macromolecules* **2007**, *40*(25), 8974–8982.
(40) Urade, V. N.; Wei, T.-C.; Tate, M. P.; Kowalski, J. D.; Hillhouse, H. W. *Chem. Mater.* **2007**, *19*(4), 768–777.

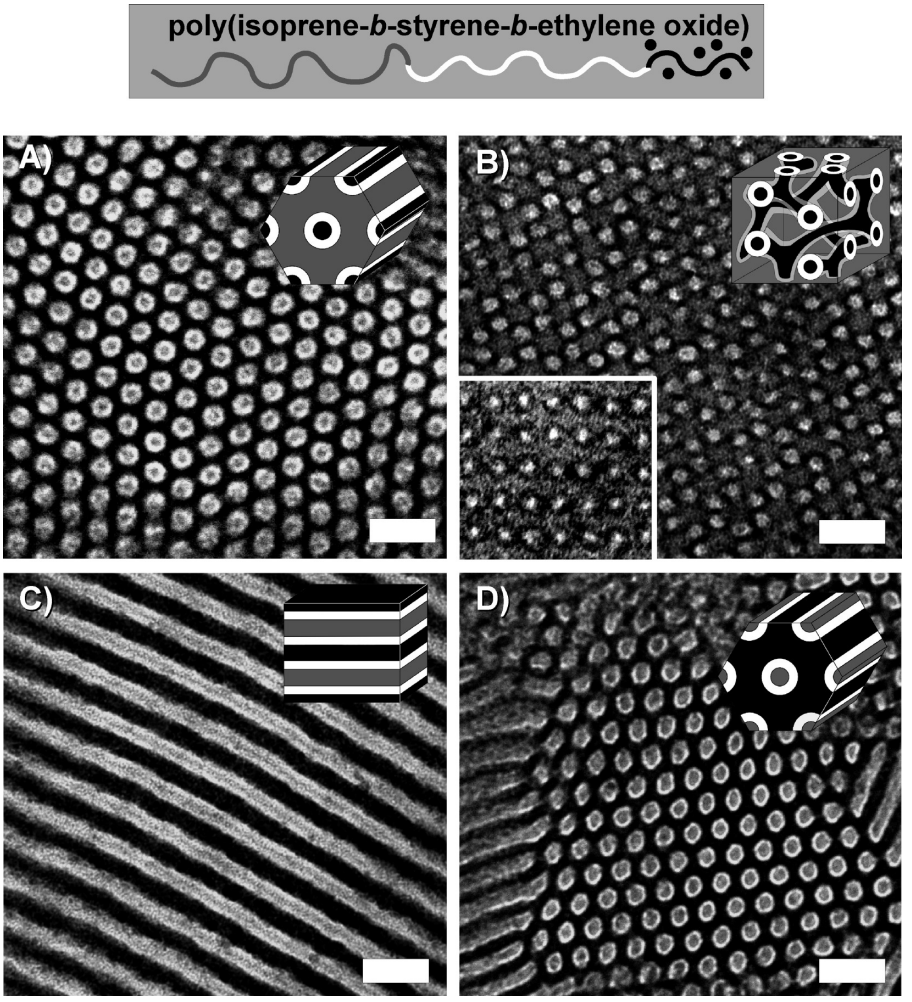

Figure 1. Representative TEM images of aluminosilicate nanocomposites with core−shell hexagonal (A) and core−shell double gyroid (B) morphologies (image and inset in B show a (111) and (100) projection, respectively). Also, representative TEM images of niobia nanocomposites with three-domain lamellae (C) and core−shell inverse-hexagonal (D) morphologies. Light regions of these images correspond to poly(styrene) and dark regions correspond to either OsO_4 stained poly(isoprene) or oxide swelled poly(ethylene oxide). The polymer schematic (top) defines the colors used in the inset morphology schematics: gray, white, and black corresponding to I, S, and O + oxide domains, respectively. Images shown at same scale with 50 nm scale bars inset. The representative TEM images above correspond to samples ISO3-S2, ISO4-S4, ISO4-N1, and ISO4-N3, respectively.

A free-standing mesoporous aluminosilicate double gyroid structure was synthesized by removing the ISO from sample ISO4-S4 using a reactive oxygen plasma. After 10 min of etching, the ISO was removed and the structure was preserved as evidenced by ordered network structures viewed on TEM (Figure 3). TEM observation of this sample revealed 5−11 nm diameter tubes of aluminosilicate with 3-fold nodes and 29 to 37 nm mesopores. The free-standing aluminosilicate structure was much more sensitive to the intensity of the incident electron bream than the nanocomposites and had to be imaged with a low intensity beam with very long CCD exposure times to limit the distortion of the structure. Furthermore, the lower contrast relative to Figure 1B is due to the much lower atomic number of silicon as compared to osmium as well as the plasma treatment leading to a much lower density than bulk aluminosilicates.

Niobia Nanocomposites. Seven additional samples were synthesized with a niobia sol in order to further explore the ISO-oxide phase diagram with the sol of a transition metal oxide. Samples spanned the $f_I = f_S$ isopleth from 43.8 to 70.0 vol % O + oxide.

Five of these niobia nanocomposites had volume fractions within the 27−62 vol % O range of the three-domain lamellae phase of neat ISO polymers along the $f_I = f_S$ isopleth.[28] Only two of the five samples with the lowest O + oxide volume fraction, ISO4-N1 and ISO4-N2, with O + oxide fractions ranging from 43.8 to 48.2 vol %, were identified to have the Lam_3 morphology by TEM and SAXS. The TEM images of these stained Lam_3 nanocomposites had layers of O + oxide (dark), S (light), and I (gray) arranged in patterns of ISO−OSI− which is characteristic of this morphology (Figure 1C). The switching of O + oxide and stained I contrast in the niobia samples is due to the much higher atomic number of Nb (41) compared to Si (14) and Al (13). This results in the niobia providing more electron scattering contrast than the OsO_4 stained I. The SAXS patterns of these two samples have peaks consistent with lamellar symmetry, with peaks at $q/q^* = 1, \sqrt{4}$, and $\sqrt{9}$ (Figure 2C). The d_1 lattice spacing measured by SAXS varied from 24.0 to 26.3 nm and was

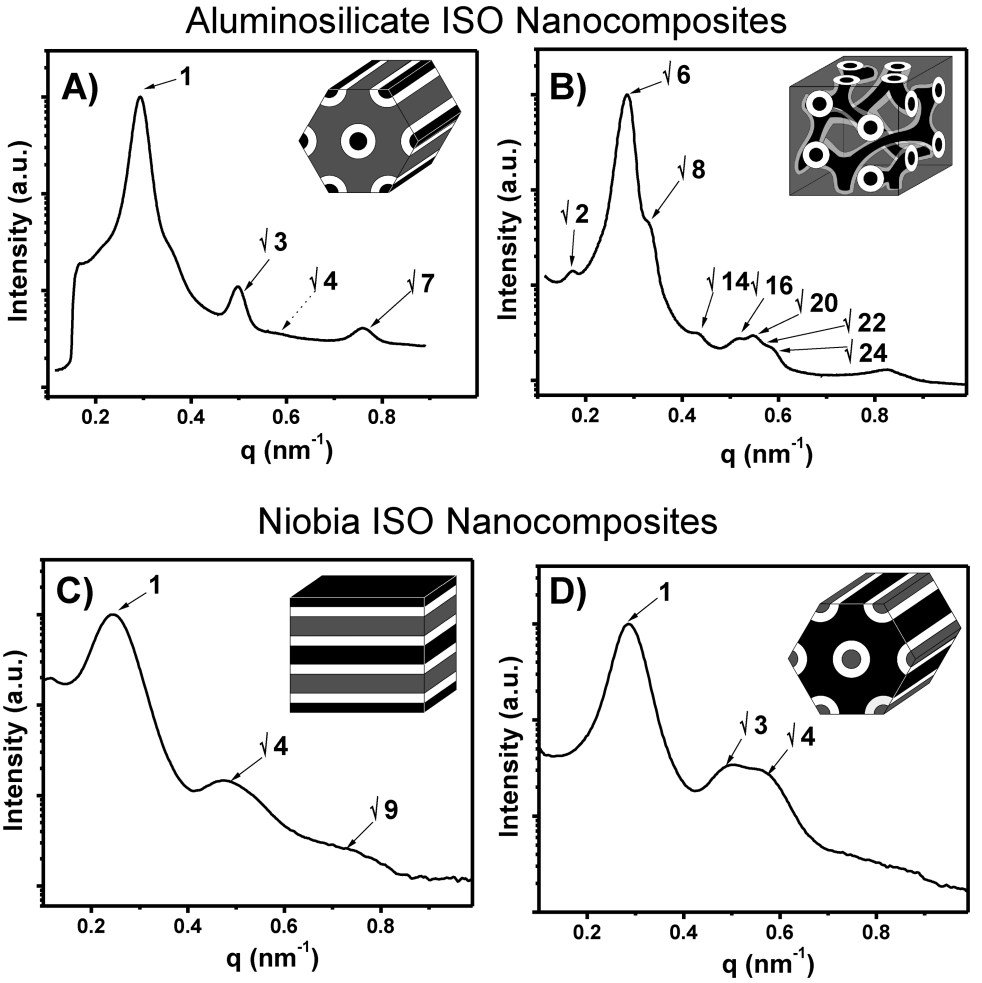

Figure 2. Representative SAXS patterns of aluminosilicate nanocomposites with core−shell hexagonal (A) and core−shell double gyroid (B) morphologies as well as niobia nanocomposites with three-domain lamellae (C) and core−shell inverse-hexagonal (D) morphologies. The sequence of expected peaks is indicated in each spectrum. The patterns correspond to samples ISO4-S2, ISO4-S3, ISO4-N1, and ISO4-N3, respectively.

Table I. Compositions, Morphologies, and *d*-Spacing of ISO + Oxide Nanocomposites

film name	v % I	v % S	v % O + oxide	morphology	*d* (nm)[a]	*d* (nm)[b]
ISO3-S1	41.9%	42.4%	15.7%	worm	21.2	18
ISO3-S2	40.5%	41.0%	18.5%	CS-H	22.2	17
ISO3-S3	38.6%	39.1%	22.3%	CS-H	21.9	19
ISO3-S4	33.6%	34.1%	32.3%	CS-G^D(Lam_3)	54.6	62
ISO4-S1	42.7%	42.3%	15.0%	CS-H (worm)	19.9	19
ISO4-S2	41.6%	41.1%	17.3%	CS-H	21.7	19
ISO4-S3	38.7%	38.3%	23.0%	CS-G^D	52.9	63
ISO4-S4	35.2%	34.8%	30.0%	CS-G^D	56.2	53
ISO3-N1	18.6%	18.9%	62.5%	[c]CS-iH	23.1	23
ISO3-N2	14.9%	15.1%	70.0%	[c]CS-iH	21.6	20
ISO4-N1	28.3%	27.9%	43.8%	Lam_3	26.3	29
ISO4-N2	26.0%	25.7%	48.2%	Lam_3	24.0	22
ISO4-N3	24.6%	24.3%	51.1%	CS-iH	22.0	23
ISO4-N4	23.1%	22.9%	54.0%	CS-iH	24.8	23
ISO4-N5	21.1%	20.9%	58.0%	[c]Lam_3	21.7	20

[a] Lattice dimensions (*d*) are based on the lamellar (1), hexagonal (10), and gyroid (100) planes calculated from $d = 2\pi/q^*$. [b] Lattice dimension determined by TEM imaging. [c] Precipitation of inorganic species leads to a morphology with a lower effective volume fraction of PEO + oxide.

consistent with both the observed c.a. 25 nm spacings observed in TEM and the molecular weight of the ISO polymer.

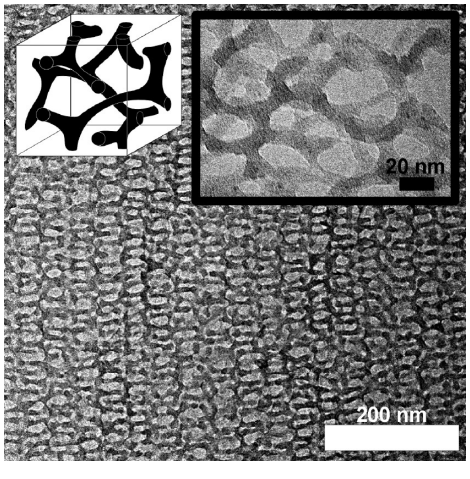

Figure 3. TEM image of free-standing mesoporous oxide double gyroid resulting from oxygen plasma removal of ISO structure directing agent from ISO4-S4. Schematic of the morphology (left inset) is next to the high magnification TEM image (right inset).

Niobia nanocomposites with O + oxide fractions beyond 50.0 vol % were found to form a different morphology. Neat ISO polymers are known to form core−shell double gyroid (Q^{230}) and core−shell hexagonal phases in narrow composition windows on the O-rich side of the

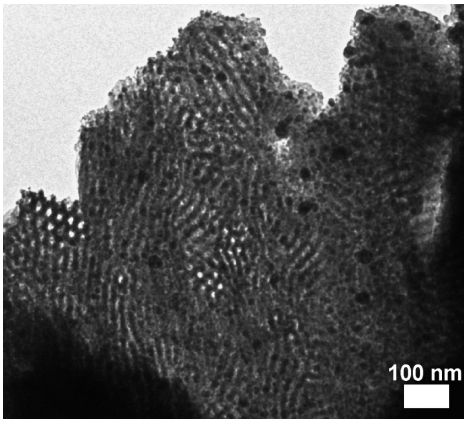

Figure 4. Representative TEM image of sample ISO3-N2 showing macrophase separation of niobia precipitates at high oxide loadings (> 58 vol % O + oxide).

ISO phase diagram.[28] Samples ISO4-N3 and ISO4-N4 had O + oxide fractions of 51.1 and 54.0 vol %, respectively, and both formed the same morphology. TEM images of these samples showed a hexagonal arrangement of continuous tubes of I (gray) covered with shells of S (white) within a matrix of O + oxide (dark) (Figure 1D). Although this image is similar to the aluminosilicate core−shell hexagonal image (compare Figure 1A and D), the I and O + oxide domains have switched places. Accordingly, this morphology is named core−shell inverse-hexagonal (CS-iH) since the O + oxide domain forms the matrix. The SAXS patterns of these two samples were also consistent with the observed hexagonal symmetry, showing scattering peaks at $q/q^* = 1$, $\sqrt{3}$, and $\sqrt{4}$ (Figure 2D). The d_{10} spacing varied from 22.0 and 24.8 nm and was consistent with c.a. 23 nm spacings observed in TEM as well as the molecular weight of the ISO polymer used.

The niobia nanocomposites synthesized with 58 vol % O + oxide or more had macrophase separated regions of niobia. Samples ISO4-N5, ISO3-N1, and ISO3-N2 all had clear formation of precipitates throughout the films when viewed on the TEM (Figure 4). The precipitation of some of the niobia sol from solution leads to a lower effective volume fraction of niobia mixed with O block of the polymer. This is likely why ISO4-N5 with 58 vol % O + oxide exhibited a Lam_3 morphology predominantly in TEM and SAXS (data not shown). Samples ISO3-N1 and ISO3-N2 also had clear macrophase separation, but still had the expected CS-iH morphology. The macrophase separation correlated to a decrease in d_{10} in the ordered regions relative to samples of similar composition (Table I).

Discussion

The morphology results of 15 oxide nanocomposites structure-directed with two different ISO triblock terpolymers along the $f_I = f_S$ isopleth are displayed in Figure 5. Due to the many parameters of this phase space, the two-dimensional ternary phase diagram represents a small slice of the complete phase space along this isopleth. In particular, the molecular weight (N) and volume fraction of O (f_O) were only varied within a narrow range. Furthermore, this morphology map is a composite containing results from both aluminosilicate and niobia nanocomposites. Each morphology is discussed separately before the overall phase behavior of this isopleth is discussed.

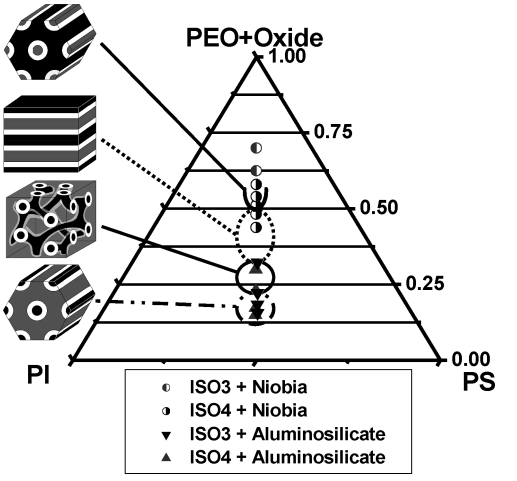

Figure 5. Morphology map for poly(isoprene-*b*-styrene-*b*-ethylene oxide) nanocomposites with axes indicating the volume fractions of I, S, and O + oxide. Symbols identify the polymer and oxide used. Four ordered morphologies were identified, including core−shell hexagonal, core−shell double gyroid, three-domain lamellae, and core−shell inverse-hexagonal. The three samples with the highest O + oxide fractions had oxide precipitation from the polymer which lead to lower effective O + oxide volume fractions.

Core−Shell Hexagonal Phase. The core−shell hexagonal phase was found to form in the composition window from 15.0 to 22.3 vol % O + oxide. This contrasts sharply from neat ISO which forms the O^{70} phase from 9.8 to 23.9 vol % O along the same isopleth. This CS-H phase was even observed when ISO4 (forms O^{70} when neat) was mixed with just 2.9 vol % aluminosilicate (ISO4-S1). Clearly, the system thermodynamics were strongly affected by the selective mixing of sol particles with the O domain. A similar suppression of the O^{70} phase was observed when relatively small amounts of lithium perchlorate were mixed with similar ISO polymers.[4] The marked change in phase behavior was attributed to the 17-fold increase in segregation strength induced by the selective dissolution of lithium perchlorate into the O blocks. An analogous effect is likely at play in the ISO-oxide system. The effect of the addition of oxide nanoparticles on the segregation strength of ISO was crudely estimated[41] by comparing the d^* ($\equiv 2\pi/q^*$) spacing of hexagonal ISO3 to that of ISO3-S2 using $d^* \propto \chi^{1/6}$. This approximation leads to an estimated increase in χ by a factor of 1.8 upon addition of oxide sol. While addition of oxide sol to ISO does not increase χ nearly as much as lithium perchlorate, it is still sufficient to explain the similar change in phase behavior. The CS-H phase was not only found at very low oxide loadings, but also into the dense nanoparticle regime.[42] Sample ISO3-S3 formed

(41) Semenov, A. N. *Macromolecules* **2002**, *22*(6), 2849–2851.
(42) Jain, A.; Wiesner, U. *Macromolecules* **2004**, *37*(15), 5665–5670.

the CS-H phase with an aluminosilicate volume fraction larger than the O vol fraction. The CS-H phase was stabilized by the increased segregation strength induced by very small amounts of oxide and was preserved into the dense nanoparticle regime.

Core−Shell Double Gyroid Phase. The core−shell double gyroid morphology was found with O + oxide volume fractions ranging from 23.0 to 32.3 vol %. This large 9.3 vol % O + oxide window is comparable to the 14.1 vol % O window for the O^{70} phase in neat ISO polymers along the same isopleth. From a synthetic standpoint, this wide phase window with ISO structure-directing agents makes the fabrication of materials with trifunctional network structures far easier than with diblock copolymers.[31] The existence of this network structure in the ISO-oxide system was quite unexpected considering the suppression of all network phases when similar ISO polymers were selectively swelled with lithium salts.[4] In this case, the less drastic increase in segregation strength for the ISO-oxide system likely leads to the replacement of O^{70} with CS-G^D rather than the complete suppression of network phases.

Three-Domain Lamellae Phase. The Lam_3 phase was found with O + oxide fractions ranging from about 32.3 to 48.2 vol %. The Lam_3 phase window for ISO-oxide is more narrow than that of neat ISO polymers (27 to 62 vol % O) but occurs over a similar region of the $f_I = f_S$ isopleth. The considerable asymmetry of the phase boundaries about the $f_I = f_S = f_O = 1/3$ symmetric point is due to the asymmetry of the I, S, and O mer units as well as the asymmetry of the χ parameters[19,43] which was exaggerated by the addition of oxide sols.

Core−Shell Inverse-Hexagonal Phase. The core−shell inverse-hexagonal morphology was found when the O + oxide composition was between 51 and 54 vol %. Larger O + oxide fractions could be explored by starting with ISO polymers with larger O fractions or perhaps by modifying the niobia sol−gel process. However, such searches toward the O + oxide rich corner of the phase diagram are likely to result in isolated micellar phases or disordered mixing. The onset of the CS-iH at 51 vol % O + oxide is considerably lower than that predicted for neat ISO polymers (c.a. 70 to 80 vol % O)[19] and is likely due to the increased segregation strength of the O + oxide domain. It is impressive to note how well the ISO−oxide system behaves deep into the dense nanoparticle regime. For example, ISO4-N4 with 54 vol % O + oxide contained 7.2 times more volume of oxide than O yet still formed a highly ordered morphology. All samples targeting O + oxide fractions higher than 54 vol % resulted in macrophase separation of niobia precipitates (ISO3-N1, ISO3-N2, and ISO4-N5). The isolated precipitates of niobia resulted in a lower effective O + oxide volume fraction. This lower effective O + oxide fraction led ISO4-N5 to form a Lam_3 phase even though the recipe targeted an O + oxide region of phase space near CS-iH. This lower effective O + oxide fraction was further evidenced in SAXS by a shift to smaller d^* spacing (compare ISO4-N4 to ISO4-N5 and ISO3-N1 to ISO3-N2).

Phases Encountered. The phase behavior observed in the ISO−oxide system was characteristic of the nonfrustrated ISO polymers used. All of the observed phases—CS-H, CS-G^D, Lam_3, and CS-iH—exhibited only A−B and B−C type interfaces without any A−C type contacts. The four observed phases were all core−shell analogs of the lamellar, double gyroid, and hexagonal phases common to diblock copolymers and appeared in same sequence. The very different phase space of the ISO−oxide system relative to neat ISO is attributed to the change in system thermodynamics which was evidenced even at very low oxide loadings.

The network morphology observed in the ISO−oxide system differed substantially from neat ISO. Along the $f_I = f_S$ isopleth, neat ISO polymers form the orthorhombic O^{70} phase on the O minority side of the isopleth from 9.8 to 23.9 vol % O and the cubic core−shell double gyroid on the O majority side of the isopleth from 61 to 67 vol % O.[28] In contrast, the ISO−oxide system differed in two regards: (1) the cubic core−shell double gyroid structure formed on the O + oxide minority side of the isopleth and (2) no network phases were found on the O + oxide majority side of the isopleth. The appearance of the CS-G^D phase on the O + oxide minority side of the isopleth (1) can be rationalized by a slight distortion of neat ISO phase boundries[19] by extending the CS-G^D phase space slightly toward the S corner of the ternary phase diagram. The change in ISO thermodynamics with the addition of oxide sol could be attributed to such a shift. As predicted for neat ISO, the symmetric−asymmetric ISO structure-directing agents lead to an ISO−oxide network structure with saddle surfaces.[26] In contrast the lack of any observed network structures on the O + oxide majority side of the isopleth (2) requires further discussion. Although the existence of an ISO−oxide network phase on the O + oxide majority side of the isopleth cannot be disproved, it is not expected for the polymers used in this study since no such phases were observed as minority phases in samples ISO4-N2 or ISO4-N3 near the transition from Lam_3 to CS-iH. We suspect that O + oxide majority network phases are suppressed by the entropic penalty associated with the O chain stretching necessary to reach the center of each node. This effect was likely exacerbated by the relatively small O fraction of the ISO polymers used in this study as well as the increased unit cell size at high oxide loadings. For comparison, such O + oxide majority network phases for IO diblock copolymers are know to form under a narrow set of conditions including a larger 32 vol % O.[31,39] Furthermore, the stability of ISO−oxide network phases may be rationalized in terms of the increased polydispersity of the combined O + oxide domain. Copolymers with blocks of different polydispersity are known to favor structures with surfaces curving

(43) Floudas, G.; Vazaiou, B.; Schipper, F.; Ulrich, R.; Wiesner, U.; Iatrou, H.; Hadjichristidis, N. *Macromolecules* **2001**, *34*(9), 2947–2957.

toward the block of higher dispersity.[44−47] Thus, the stability of O + oxide minority network phases is expected to be higher than that of O + oxide majority network phases. There is likely a narrow set of conditions under which the ISO−oxide system forms network phases on the O + oxide majority side of the $f_I = f_S$ isopleth; however, we do not expect these conditions to be as experimentally tractable as when O + oxide is a minority.

Outlook for Applications. The reported CS-H, CS-G^D, Lam_3, and CS-iH morphologies could be useful for applications requiring continuous paths of multiple functional materials. The core−shell hexagonal morphologies contain a continuous matrix with two minority components that are continuous in one dimension whereas the Lam_3 phase has all three components continuous in two dimensions. In contrast, the CS-G^D morphology has a pentacontinuous structure with all five-plies continuous in all directions. A series of selective domain transformations[48−50] could be used to convert the materials reported here into nanocomposites containing multiple function materials with either anisotropic or isotropic continuity. Such materials could be useful for advanced applications including photonic materials as well as energy generation, conversion, and storage devices.

Furthermore, ordered materials with continuous porosity are of interest for filtration, electronic, and optical applications. Toward this end, we demonstrated a free-standing mesoporous aluminosilicate double gyroid (Figure 3). Such materials could be directly used as orientation independent filters. Alternatively, these free-standing oxide networks could be used as sacrificial hard templates for the synthesis of mesoporous, crystalline transition metal oxides.[51] Similarly, these oxide networks could also be used as substrates for the deposition of layers of functional materials for three-dimensionally continuous electronic and optical devices.

Conclusion

The results of 15 ISO−oxide nanocomposites were detailed along the $f_I = f_S$ isopleth using aluminosilicate and niobia sols. Four morphologies were identified, including core−shell hexagonal, core−shell double gyroid, three-domain lamellae, and core−shell inverse-hexagonal. These three- and five-ply nanocomposites contained continuous domains spanning in either one, two, or three dimensions. We believe that this approach will lead to advanced materials and devices containing several plies of functional materials.

Acknowledgment. This work was supported by the Cornell Fuel Cell Institute via the Cornell Center for Materials Research, a Materials Research Science and Engineering Center of the National Science Foundation (NSF DMR-0520404). This publication was further supported by a Grant Number R21DE018335 from the National Institute of Dental and Craniofacial Research. This work was supported at the University of Minnesota by the NSF (DMR 0220460 and by the MRSEC Program of the National Science Foundation under Award Number DMR-0212302 and DMR-0819885). This work made use of the Cornell Center for Materials Research Shared Facilities, supported through the NSF Materials Research Science and Engineering Centers program. The X-ray equipment was supported by Department of Energy grant DEFG-02-97ER62443. CHESS was supported by the NSF and NIH-NIGMS via DMR-0225180.

(44) Lynd, N. A.; Hillmyer, M. A. *Macromolecules* **2005**, *38*(21), 8803–8810.
(45) Cooke, D. M.; Shi, A. C. *Macromolecules* **2006**, *39*(19), 6661–6671.
(46) Ruzette, A. V.; Tence-Girault, S.; Leibler, L.; Chauvin, F.; Bertin, D.; Guerret, O.; Gerard, P. *Macromolecules* **2006**, *39*(17), 5804–5814.
(47) Meuler, A. J.; Ellison, C. J.; Qin, J.; Evans, C. M.; Hillmyer, M. A.; Bates, F. S. Polydispersity effects in poly(isoprene-b-styrene-b-ethylene oxide) triblock terpolymers. *J. Chem. Phys.* **2009**, *130*(23), 234903-1−234903-17.
(48) Hillmyer, M. A. *Block Copolymers II* **2005**, *190*, 137–181.
(49) Ryoo, R.; Joo, S. H.; Jun, S. *J. Phys. Chem. B* **1999**, *103*(37), 7743–7746.
(50) Lee, J.; Yoon, S.; Hyeon, T.; Oh, S. M.; Kim, K. B. *Chem. Commun.* **1999**, No. 21, 2177–2178.
(51) Tian, B.; Liu, X.; Solovyov, L. A.; Liu, Z.; Yang, H.; Zhang, Z.; Xie, S.; Zhang, F.; Tu, B.; Yu, C.; Terasaki, O.; Zhao, D. *J. Am. Chem. Soc.* **2003**, *126*(3), 865–875.